Guided Wave Propagation in an Elastic Hollow Cylinder Coated with a Viscoelastic Material

James N. Barshinger, *Member, IEEE*, and Joseph L. Rose, *Member, IEEE*

***Abstract*—The propagation of ultrasonic guided waves in an elastic hollow cylinder with a viscoelastic coating is studied. The principle motivation is to provide tools for performing a guided wave, nondestructive inspection of piping and tubing with viscoelastic coatings. The theoretical boundary value problem is solved that describes the guided wave propagation in these structures for the purpose of finding the guided wave modes that propagate with little or no attenuation. The model uses the global matrix technique to generate the dispersion equation for the longitudinal modes of a system of an arbitrary number of perfectly bonded hollow cylinders with traction-free outer surfaces. A numerical solution of the dispersion equation produces the phase velocity and attenuation dispersion curves that describe the nature of the guided wave propagation. The attenuation dispersion curves show some guided wave modes that propagate with little or no attenuation in the coated structures of interest. The wave structure is examined for two of the modes to verify that the boundary conditions are satisfied and to explain their attenuation behavior. Experimental results are produced using an array of transducers positioned circumferentially around the pipe to evaluate the accuracy of the numerical solution.**

I. Introduction

Many researchers have been interested in the application of ultrasonic guided waves for the nondestructive inspection of tubes and pipes [1]–[4]. They have recognized the possibility for rapid, accurate, and inexpensive nondestructive assessment of these structures that exist in the infrastructure of many industries, such as oil, gas, and water transport; power generation; and chemical processing. One of the potential difficulties in inspecting these structures is the presence of viscoelastic coatings that are commonly used for corrosion protection. These coatings tend to attenuate the propagating energy and can severely degrade the performance of a guided wave test with regard to test sensitivity and the distance of propagation.

One of the proposed solutions to this problem has been to perform the inspection using the lowest order longitudinal or torsional modes at low excitation frequencies in which guided waves will penetrate coated structures; often as low as 30 kHz for the longitudinal mode, and as low as 8 kHz for the torsional mode [4]. Although this method produces propagating wave modes that will penetrate the coated structure, the sensitivity of the test to finding small defects can be severely compromised because the wavelength of the guided wave mode becomes on the order of, or significantly larger than, the size of the defects that are typically being sought.

Alternatively, there is the possibility that, for viscoelastic coated structures, there are certain higher order mode and frequency choices that have the modal characteristics necessary to propagate with less attenuation than others in which defect detection is not compromised. This is due to the abundance of mode choices, each having a unique stress and displacement characteristic, wave structure, in the wave guide [5]. One way to determine these modes would be a trial-and-error method of tuning generation parameters such as the transducer incident angle and frequency to find the modes with the least attenuation. Although this method can be effective, the associated time and equipment cost can make it impractical. Therefore, a theoretical model of the coated structure to predict attenuation characteristics is a more attractive method for finding suitable modes for a guided wave inspection [6]–[8].

Manuscript received November 11, 2003; accepted April 6, 2004.

J. N. Barshinger is with General Electric Global Research Center, Nondestructive Technologies Lab, Niskayuna, NY (barshing@crd.ge.com).

J. L. Rose is with Engineering Science and Mechanics, The Pennsylvania State University, University Park, PA.

II. Theory

A. Background

The initial analysis of elastic wave propagation in wave guides was carried out in the late 19th and early 20th centuries by researchers studying elastic wave propagation for various geometrical wave-guide shapes. Rayleigh [9] and Lamb [10] studied the elastic wave propagation in traction-free, isotropic plates. Pochhammer [11] and Chree [12] studied the elastic wave propagation in infinitely long cylindrical rods. Early efforts also were presented for the analysis of hollow cylinders by using shell theory approximations and assuming axially symmetric motion such as Love [13] and Rayleigh [9]. Other researchers such as Lin and Morgan [14], Cooper and Naghdi [15], and Mirsky and Herrmann [16], [17], also used shell theories to solve for the frequency/wave number relationships for axisymmetric motion of hollow cylinders. In 1959, Gazis [18], [19] developed an exact elastic solution for a hollow cylinder, including axially symmetric, nonaxially symmetric, and torsional wave modes.

The earliest works for multilayer elastic wave guides using matrix techniques was presented by Thomson [20],

Haskell [21], and Knopoff [22] to model seismological effects in the layered structure of the earth. Viscoelastic and leakage effects also have been included by various researchers to model the attenuation behavior of guided wave modes [23]–[25]. Lowe [26] presents an excellent summary of the use of matrix techniques to model multilayered structures. In addition to a general overview of the formulation of multilayer problems, he presents some insights on performing the numerical solution of the dispersion equation. Particularly, he uses functional minimization to solve the complex roots of the dispersion equation for systems, including material damping.

Many general references for wave propagation theory exist, such as Viktorov [27], Graff [28], Achenbach [29], Auld [30], Rose [31] and others. Ewing *et al.* [32] is also a good general reference for wave propagation in multilayered media. Some additional references for the viscoelastic model and coated shells are [33], [34].

B. Axially Symmetric Waves in a Cylindrical Shell

For a homogeneous, isotropic medium, the vector form of Navier's equation of motion is:

$$\mu\nabla^2\mathbf{u} + (\lambda+\mu)\nabla(\nabla\cdot\mathbf{u}) = \rho\frac{\partial^2\mathbf{u}}{\partial t^2}, \tag{1}$$

where $\mathbf{u}$ is the displacement field, λ and μ are the Lamé constants for the material, and ρ is the density. To obtain a solution for (1), the displacement field is assumed to be a combination of the gradient of a scalar potential field, Φ, and the curl of a vector potential field, $\mathbf{H}$, with the additional constraint that $\nabla\cdot\mathbf{H}=0$ [28]:

$$\mathbf{u} = \nabla\Phi + \nabla\times\mathbf{H}. \tag{2}$$

Substitution of (2) into (1) results in scalar and vector wave equations:

$$\nabla^2\Phi = \frac{1}{c_1^2}\frac{\partial^2\Phi}{\partial t^2},\quad c_1=\sqrt{(\lambda+2\mu)/\rho}, \tag{3}$$

$$\nabla^2\mathbf{H} = \frac{1}{c_2^2}\frac{\partial^2\mathbf{H}}{\partial t^2},\quad c_2=\sqrt{\mu/\rho}, \tag{4}$$

Eq. (3) represents the longitudinal wave motion in the structure and (4) represents the shear wave motion, c_1 and c_2 are the longitudinal and shear wave velocities of the medium. The vector potential field, $\mathbf{H}$, is composed of scalar components H_r, H_θ, and H_z.

In order to consider the complete solution for the wave propagation in the structure, including axially symmetric, nonaxially symmetric, and torsional modes, the two wave equations must be solved entirely [18], [19]. However, to obtain the longitudinal guided-wave modes, the axially symmetric solution can be isolated by setting the H_r and H_z components of the vector potential to be zero. The remaining component, H_θ, and the scalar potential, Φ, must only be a function of coordinates r and z [28]. Considering the elimination of two components of the vector potential, and the restrictions on the other component, the wave equation for the shear motion becomes a scalar wave equation in H_θ:

$$\nabla^2 H_\theta - \frac{H_\theta}{r^2} = \frac{1}{c_2^2}\frac{\partial^2 H_\theta}{\partial t^2}. \tag{5}$$

To solve the two scalar wave equations, assume harmonic wave propagation in the positive z coordinate direction such that the solutions are of the following form:

$$\Phi = f(r)e^{i(kz-\omega t)}, \tag{6}$$

$$H_\theta = h(r)e^{i(kz-\omega t)}. \tag{7}$$

Substituting (6) into (3) yields a form of Bessel's equation:

$$r^2f'' + rf' + r^2\alpha^2 f = 0;\ \ \alpha^2 = (\omega^2/c_1^2 - k^2). \tag{8}$$

Eq. (8) has a solution that can be expressed in terms of zeroth order Hankel functions:

$$f(r) = A_{(L+)}H_0^1(\alpha r) + A_{(L-)}H_0^2(\alpha r). \tag{9}$$

Substituting (7) into (5) also yields a form of Bessel's equation:

$$r^2h'' + rh' + \left\{r^2\beta^2 - 1\right\}h = 0;\ \ \beta^2 = (\omega^2/c_2^2 - k^2). \tag{10}$$

Eq. (10) has a solution that can be expressed in terms of first order Hankel functions:

$$h(r) = A_{(S+)}H_1^1(\beta r) + A_{(S-)}H_1^2(\beta r). \tag{11}$$

Substituting (9) and (11) into (6) and (7), the solutions for the scalar and vector fields are:

$$\Phi = \left\{A_{(L+)}H_0^1(\alpha r) + A_{(L-)}H_0^2(\alpha r)\right\}e^{i(kz-\omega t)}, \tag{12}$$

$$\mathbf{H} = \left\{A_{(S+)}H_1^1(\beta r) + A_{(S-)}H_1^2(\beta r)\right\}e^{i(kz-\omega t)}\mathbf{e}_\theta. \tag{13}$$

The choice of Hankel functions as opposed to Bessel functions is important in obtaining a numerically stable solution in regions in which the argument of the functions becomes imaginary. These solution regions occur for values of wave number in which the longitudinal or shear wave components in the individual layers become nonpropagating (i.e., when a critical angle is exceeded).

Physically, the Hankel functions individually represent the propagating longitudinal and shear waves in the layer [28], such that the unknown amplitude constants for each term are described with the subscripts (L) and (S) to denote longitudinal and shear waves, and $(+)$ and $(-)$ to indicate propagation in the outward and inward directions, respectively.

When substituted into (2), (12) and (13) yield a solution to the displacement equation of motion in terms of the unknown amplitude constants for longitudinal and

shear waves propagating in the structure. The individual, nonzero displacement components are:

$$u_r = \begin{Bmatrix} A_{(L+)}\left[-\alpha H_1^1(\alpha r)\right] + A_{(L-)}\left[-\alpha H_1^2(\alpha r)\right] \\ +A_{(S+)}\left[kH_1^1(\beta r)\right] + A_{(S-)}\left[kH_1^2(\beta r)\right] \end{Bmatrix} e^{i(kz-\omega t)}, \tag{14}$$

$$u_z = \begin{Bmatrix} A_{(L+)}\left[-kH_0^1(\alpha r)\right] + A_{(L-)}\left[-kH_0^2(\alpha r)\right] \\ +A_{(S+)}\left[-\beta H_0^1(\beta r)\right] + A_{(S-)}\left[-\beta H_0^2(\beta r)\right] \end{Bmatrix} e^{i(kz-\omega t)}. \tag{15}$$

The stresses in the layer can be derived with respect to the unknown amplitude constants by first using the strain-displacement constitutive equations, then the stress-strain constitutive equations from linear elastic theory.

$$\sigma_{rr} = \mu \begin{Bmatrix} A_{(L+)}\left[(k^2-\beta^2)H_0^1(\alpha r) + 2\frac{\alpha}{r}H_1^1(\alpha r)\right] \\ +A_{(L-)}\left[(k^2-\beta^2)H_0^2(\alpha r) + 2\frac{\alpha}{r}H_1^2(\alpha r)\right] \\ +A_{(S+)}\left[2k\beta H_0^1(\beta r) - 2\frac{k}{r}H_1^1(\beta r)\right] \\ +A_{(S-)}\left[2k\beta H_0^2(\beta r) - 2\frac{k}{r}H_1^2(\beta r)\right] \end{Bmatrix} e^{i(kz-\omega t)}, \tag{16}$$

$$\sigma_{rz} = \mu \begin{Bmatrix} A_{(L+)}\left[-2k\alpha H_1^1(\alpha r)\right] \\ +A_{(L-)}\left[-2k\alpha H_1^2(\alpha r)\right] \\ +A_{(S+)}\left[(k^2-\beta^2)H_1^1(\beta r)\right] \\ +A_{(S-)}\left[(k^2-\beta^2)H_1^2(\beta r)\right] \end{Bmatrix} e^{i(kz-\omega t)}. \tag{17}$$

C. The Global Matrix Method

The next step in obtaining the dispersion equation for the multilayer structure is to develop the expressions for the boundary conditions of the layer system. Matrix methods have been recognized as being an excellent tool for assembling these expressions [20]–[22], [26]. The general methodology is to formulate a matrix/vector representation of the stress and displacement variables that are needed for the boundary conditions. A global matrix then can be derived from the individual matrix equations for each interface or boundary condition. This global matrix developed through the assembly of the entire set of boundary conditions for the multilayer system. Because it is just as easy to develop the equations for an arbitrary number of layers as it is to generate the equations for a two-layer system, the more general case is developed here.

Fig. 1 shows a wave guide consisting of n cylindrical layers perfectly bonded together with traction-free surfaces at the inner and outer interfaces of the entire system. Each layer is homogeneous and isotropic so that each is governed by the equations that have been developed thus far. The boundary conditions at the traction-free surfaces are the vanishing of normal and shear stresses and are given by:

$$\begin{Bmatrix} \sigma_{rr} \\ \sigma_{rz} \end{Bmatrix}_{\substack{\text{Free} \\ \text{Surface}}} = 0. \tag{18}$$

The interfacial continuity condition at the joining between two perfectly bonded layers is the continuity of displacement components and the normal and shear components of stress. For instance, the boundary condition between arbitrary layers i and $(i+1)$ is:

$$\begin{Bmatrix} u_z \\ u_r \\ \sigma_{rr} \\ \sigma_{rz} \end{Bmatrix}_{\substack{\text{Layer}=i \\ \text{Interface}=i+1}} = \begin{Bmatrix} u_z \\ u_r \\ \sigma_{rr} \\ \sigma_{rz} \end{Bmatrix}_{\substack{\text{Layer}=i+1 \\ \text{Interface}=i+1}}. \tag{19}$$

A matrix/vector expression for the displacements and stresses of interest at an arbitrary position in a cylindrical layer can be written from (14)–(17) as:

$$\begin{Bmatrix} u_z \\ u_r \\ \sigma_{rr} \\ \sigma_{rz} \end{Bmatrix} = [\Lambda] \begin{Bmatrix} A_{(L+)} \\ A_{(L-)} \\ A_{(S+)} \\ A_{(S-)} \end{Bmatrix} e^{i(kz-\omega t)}, \tag{20}$$

where the terms of the layer matrix, $[\Lambda]$, are:

$$\begin{aligned}
\Lambda_{11} &= -kH_0^1(\alpha r) \\
\Lambda_{12} &= -kH_0^2(\alpha r) \\
\Lambda_{13} &= -\beta H_0^1(\beta r) \\
\Lambda_{14} &= -\beta H_0^2(\beta r) \\
\Lambda_{21} &= -\alpha H_1^1(\alpha r) \\
\Lambda_{22} &= -\alpha H_1^2(\alpha r) \\
\Lambda_{23} &= kH_1^1(\beta r) \\
\Lambda_{24} &= kH_1^2(\beta r) \\
\Lambda_{31} &= \mu((k^2-\beta^2)H_0^1(\alpha r) + 2\alpha H_1^1(\alpha r)/r) \\
\Lambda_{32} &= \mu((k^2-\beta^2)H_0^2(\alpha r) + 2\alpha H_1^2(\alpha r)/r) \\
\Lambda_{33} &= \mu(2k\beta H_0^1(\beta r) - 2kH_1^1(\beta r)/r) \\
\Lambda_{34} &= \mu(2k\beta H_0^2(\beta r) - 2kH_1^2(\beta r)/r) \\
\Lambda_{41} &= -2\mu k\alpha H_1^1(\alpha r) \\
\Lambda_{42} &= -2\mu k\alpha H_1^2(\alpha r) \\
\Lambda_{43} &= \mu(k^2-\beta^2)H_1^1(\beta r) \\
\Lambda_{44} &= \mu(k^2-\beta^2)H_1^2(\beta r).
\end{aligned} \tag{21}$$

In order to apply (20) to the boundary conditions for the system, the layer matrix must be evaluated at the inside and outside interfaces for each layer. This is done by inserting the density, and material velocities, for the layer and the radius for the interface of interest into the expression for the layer matrix. The notation prescribed to these new matrices is $[\Lambda_{ij}]$ for the layer matrix evaluated for the i^{th} layer at the j^{th} interface. Furthermore, it is possible to define a new matrix $[\Gamma]$ that is simply a 2×4 matrix consisting of the lower two rows of $[\Lambda]$. This new matrix is necessary because the boundary condition equations at a free surface only involve the stress quantities. Now, the boundary condition for the two free surfaces of the system can be written as:

$$[\Gamma_{11}]\{A_1\} = \{0\}, \tag{22}$$

$$[\Gamma_{n(n+1)}]\{A_n\} = \{0\}. \tag{23}$$

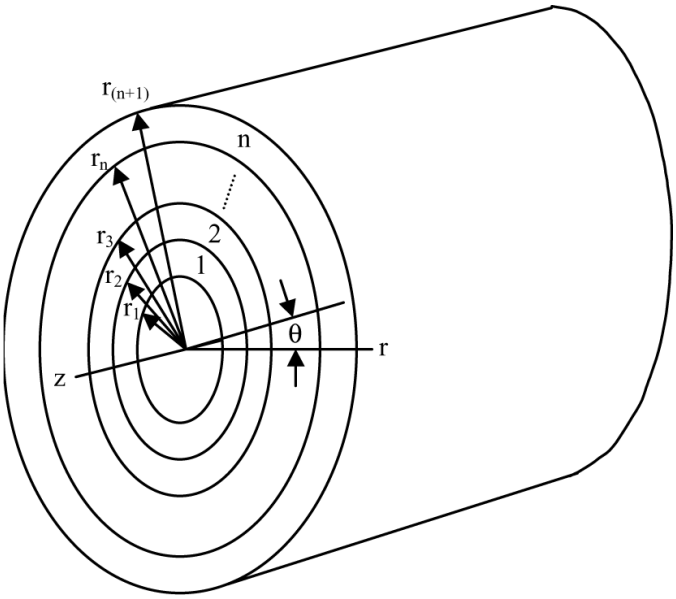

Fig. 1. Schematic representation of a system of n cylindrical layers. The cylinders are assumed to be isotropic and perfectly bonded. The internal surface of the innermost layer and the external surface of the outermost layer are assumed to be traction free. The size and material composition of the individual cylindrical layers are assumed to be arbitrary at this point.

The boundary condition at the interface between arbitrary layers, i, and $(i+1)$ is:

$$\left[\Lambda_{i(i+1)}\right]\left\{A_n\right\} = \left[\Lambda_{(i+1)(i+1)}\right]\left\{A_{(i+1)}\right\}. \tag{24}$$

This equation can be rewritten by bringing all nonzero terms to the left-hand side of the equation.

$$\left[\Lambda_{i(i+1)}\right]\left[-\Lambda_{(i+1)(i+1)}\right]\begin{Bmatrix}\{A_i\}\\ \{A_{(i+1)}\}\end{Bmatrix} = 0. \tag{25}$$

The expressions in (22), (23), and (25) can be used to assemble all of the boundary conditions for a system of n cylindrical layers. The boundary condition set then must be assembled into the form of:

$$[\Delta]\{A\} = 0, \tag{26}$$

where $[\Delta]$ is the global matrix and $\{A\}$ is a vector containing all of the unknown amplitude constants for each of the layers. As an example, for a system of four layers, the global matrix is:

$$\Delta = \begin{bmatrix} [\Gamma_{11}] & 0 & 0 & 0 \\ [\Lambda_{12}] & [-\Lambda_{22}] & 0 & 0 \\ 0 & [\Lambda_{23}] & [-\Lambda_{33}] & 0 \\ 0 & 0 & [\Lambda_{34}] & [-\Lambda_{44}] \\ 0 & 0 & 0 & [\Gamma_{45}] \end{bmatrix}. \tag{27}$$

It is easy to see how this method allows the assembly of an arbitrary system of layers. Liquid layers, as well as bulk media on the inside or outside of surfaces of the layer system, also can be handled with slight modifications of the layer matrices and the global matrix. See [31] for instance.

To obtain the modal solution for the multilayer structure, the determinant of the global matrix is set to zero, solving for the frequency and wave number values that are roots of the system of equations.

D. Viscoelastic Layers

Assuming linear viscoelasticity, and referring to Christensen [35] for the time harmonic case, elastic and viscoelastic solutions are identical, with the exception that the viscoelastic material constants are complex and frequency dependent. Thus, Navier's equation of motion for the viscoelastic case can be expressed as:

$$\mu(i\omega)\nabla^2\mathbf{u} + (\lambda(i\omega) + \mu(i\omega))\nabla(\nabla\cdot\mathbf{u}) = \rho\frac{\partial^2\mathbf{u}}{\partial t^2}, \tag{28}$$

where the Lamé constants are complex and frequency dependent. The solution to this equation for axially symmetric motion in a cylindrical shell is identical to the solution derived previously for elastic materials, except that the material constants that are introduced as wave velocities are now complex and frequency dependent (because the wave velocities are functions of the complex and frequency dependent Lamé constants). Thus, in terms of the dispersion equation, the treatment of elastic and viscoelastic layers is identical, except for the real or complex valued material constants that are input to the layer matrices.

Unlike elastic properties, there are no extensive sources for viscoelastic properties. Furthermore, the properties that can be found are typically for the frequency ranges associated with static and dynamic problems, not wave propagation problems. Therefore, it is necessary to make some sort of measurement of the viscoelastic constants at ultrasonic frequencies [36].

First, consider the equation for one-dimensional wave propagation in x, for the displacement, u, where C is the velocity of propagation as defined by (3) and (4), depending on whether longitudinal or shear wave measurements are being made. Note that the velocity is specified to be complex and frequency dependent due to the viscoelastic material properties:

$$\frac{d^2u}{dx^2} = \frac{1}{c(i\omega)^2}\frac{d^2u}{dt^2}. \tag{29}$$

Two quantities, $c(\omega)$ and $\alpha(\omega)$ can be defined from the wave velocity as follows:

$$\overline{c}(\omega) = \left(\mathrm{Re}\left(\frac{1}{c(i\omega)}\right)\right)^{-1}, \tag{30}$$

$$\alpha(\omega) = \omega\,\mathrm{Im}\left(\frac{1}{c(i\omega)}\right). \tag{31}$$

Such that the complex velocity can be expressed in terms of these constants as:

$$c(i\omega) = \left[\frac{1}{\overline{c}(\omega)} + i\frac{\alpha(\omega)}{\omega}\right]^{-1}. \tag{32}$$

The quantity $\alpha(\omega)$ is the attenuation constant and $c(\omega)$ is the phase velocity. The solution to (29) in terms of the attenuation and phase velocity is:

$$u(x,t) = De^{-\alpha(\omega)x}e^{i\omega\left(\frac{x}{c(\omega)}-t\right)}. \tag{33}$$

It is readily apparent that, for wave propagation in a viscoelastic medium, the solution involves not only a harmonic wave propagation term, but also a decaying exponential term that will cause attenuation of the propagating waves. The attenuation term is the fundamental difference between wave propagation in elastic and viscoelastic media. Losses in purely elastic media are due to geometrical spreading of the wave front and scattering, and losses in a viscoelastic material are due to those same factors with the addition of material attenuation. This is essentially a phenomenon of converting the mechanical energy of the propagating wave into heat.

Now, it is necessary to make a physical measurement of the quantities $\alpha(\omega)$ and $c(\omega)$ for both longitudinal and shear waves, at the ultrasonic frequencies of interest, so that the complex wave velocities can be obtained from (30) and (31) and are available for input to the appropriate layer matrices. The attenuation constant is measured by comparing the amplitude of longitudinal and shear waves propagating through material specimens of two different thicknesses. From (33), the ratio of amplitudes of the envelope of the received signal is:

$$\frac{A_1(x_1,\omega)}{A_2(x_2,\omega)} = e^{-\alpha(\omega)[x_1-x_2]}. \tag{34}$$

Taking the natural logarithm of both sides and rearranging yields, an expression for the attenuation constant:

$$\alpha(\omega) = -\frac{1}{x_1-x_2}\ln\left(\frac{A_1(x_1,\omega)}{A_2(x_2,\omega)}\right). \tag{35}$$

The phase-velocity measurement is done simply with a two point velocity measurement:

$$c(\omega) = \frac{x_1-x_2}{t_1(x_1,\omega)-t_2(x_2,\omega)}, \tag{36}$$

where t_1 and t_2 are the propagation times for thickness x_1 and x_2, respectively. It should be noted that (35) and (36) as written must be used in time domain with narrow band signals, and that the frequency must be incremented across the range of interest. Alternatively, broadband ultrasonic signals can be used to make the measurements of the constants by performing a Fourier transform on the signal and using (35) to obtain the attenuation constant with the amplitude information. In general, the phase information is not useful for a velocity measurement because the difference in thickness between specimens is usually many wavelengths. For the materials measured for this work, the velocity was not found to vary measurably with frequency, so broadband pulses could be used with (36) to measure the velocity.

TABLE I
ELASTIC AND VISCOELASTIC MATERIAL CONSTANTS.

Material	c_1 (km/s)	α_1/ω (s/km)	c_2 (km/s)	α_2/ω (s/km)	ρ (gm/cm^3)
Aluminum	6.33		3.13		2.70
Steel	5.90		3.19		7.80
Rexalite	2.33	0.0010	1.16	201E-8	1.05
E&C 2057 Epoxy	2.96	0.0047	1.45	0.0069	1.60
Mereco 303 Epoxy	2.39	0.0070	0.99	0.0201	1.08
Bitumastic 50 Coating	1.86	0.0230	0.75	0.2400	1.50

In order to obtain stable measurements of the attenuation constant, a through transmission water immersion fixture using Krautkramer broadband longitudinal wave transducers was used to make the measurements. Measurements were taken with 1 MHz, 2.25 MHz, and 5.0 MHz transducers, separated at a distance of 20 mm. In order to make the shear wave measurement, the specimen was placed at an incident angle to the beams to create a 45 degree refracted shear wave in the part. Note that, because the transducers in the immersion fixture were held at a constant distance, (36) was modified to be:

$$c(\omega) = \frac{x_1-x_2}{t_1-t_2+(x_1-x_2)/c_w}, \tag{37}$$

to account for the varying amount of water path.

Material constants were measured for two elastic and four viscoelastic materials as shown in Table I. Because bituminous pipe coatings are the primary interest for the industrial application of guided-wave inspection, a commercial pipe coating was obtained and measured. Table I shows the material constants for the steel pipe (elastic) and the bitumen (viscoelastic).

E. Numerical Solution

Aside from the material constants that are input to the layer matrices to form the dispersion equation, there are two unknown variables: frequency, ω, and wave number, k. Thus, to obtain a solution to the dispersion equation, one of the quantities must be held constant while solving for the other. Because analytical solutions are not available for the dispersion equation, numerical routines must be used to obtain these roots.

The plot of the wave number roots versus frequency is called the dispersion curve for the wave guide. It also is useful to convert the wave number roots to phase and group velocities and plot these quantities versus frequency resulting in phase and group velocity dispersion curves.

In general, the roots of the dispersion equations can be real, imaginary, or complex [24]. A purely real result describes a wave mode propagating with no attenuation, and it is the result typically sought for single or multilayered wave guides consisting only of elastic materials. A purely

imaginary result describes a nonpropagating, or evanescent wave mode [37], [38]. This is essentially a mode that is critically damped and thus does not propagate. This result can be important for describing stress fields very close to the wave source, but it is unimportant in the far field. Complex roots describe a propagating wave mode that is attenuating with distance from the source. This is the type of result that is of interest for viscoelastic or combination elastic/viscoelastic wave guides, and it describes the attenuation that is found for guided-wave modes propagating in such structures. This attenuation becomes readily apparent by substituting a complex wave number into the expressions for displacement or stress, that will thus have the form of (38), having both a time harmonic term in the solution and a damped exponential term that describes the attenuation of the propagating wave:

$$u, \sigma = A_{(L,S)} f(r, k, c_1(i\omega), c_2(i\omega)) e^{i(\mathrm{Re}(k)z - \omega t)} e^{-\mathrm{Im}(k)z}. \tag{38}$$

The calculation of the roots of the dispersion equation often can be quite difficult because the function is multivalued and in general quite volatile, especially in the region of wave numbers in which layers become nonpropagating, i.e., when the angle of waves striking an interface exceeds the critical angle of the adjacent layer. When considering purely elastic wave guides, a bisection routine often is used in conjunction with incremental starting values to obtain the dispersion curve roots for systems with elastic layers only. Although this method is slower in obtaining the roots than slope-following routines such as Newton's method, it is more reliable given the fact that slope-following routines often extrapolate wildly making it almost impossible to find all of the wave number roots for a given frequency. Without obtaining the complete set of roots, at many frequencies, it is difficult to plot a meaningful dispersion curve.

When considering wave guides that contain at least one viscoelastic layer, it is necessary to solve the dispersion equation for complex roots. One of the ways for finding these complex phase velocity and attenuation roots is to use a root-solving routine such as Muller's method. Unfortunately, this type of method is also a slope-following type of routing and, therefore, has the same problem as using Newton's method for finding the roots for an elastic wave guide, often extrapolating wildly and making it difficult to obtain the entire set of roots. Unfortunately, no method for complex roots is comparable to the bisection routine for real roots. An alternative method for solving the roots of the viscoelastic dispersion equation is to consider the absolute value of the function. This reduces the problem to three dimensions in which the minima represent the complex roots of the dispersion equation [26].

In order to make successful use of a minimization routine for finding the complex roots of the dispersion equation, it is necessary to have starting values that are sufficiently close to the root. Appropriate starting values for a minimization routine can be found by making the assumption that a phase-velocity root can be found on the surface of the function that is sloping toward its root by solving the dispersion equation for the elastic system of equations by temporarily setting the attenuation constants of the viscoelastic layers to zero. This real root is found with the conventional method of bisection. The real root then can be used as starting points for a search of the minimum value of the viscoelastic dispersion equation along the attenuation axis, choosing an attenuation value of zero as the starting point. The final step is to initiate a two-dimensional search in phase velocity and attenuation for the root of the viscoelastic dispersion equation using a simplex type of searching algorithm. This routine proved to be relatively robust and was adequate for calculating enough roots to create a dispersion equation. In the event that the routine missed roots along a particular mode, linear interpolation to fill for the missing values.

III. Results

A number of numerical and experimental observations were made to explore the nature of wave propagation in an elastic hollow cylinder coated with a viscoelastic material. Numerically, a computer program was written in Matlab (The MathWorks, Inc., Natick, MA) to implement the previously described root-finding routine to calculate the roots of the dispersion equation for a multilayered, hollow cylinder with viscoelastic layers. Phase velocity and attenuation dispersion curves were calculated for a 4 in. Schedule 40 steel pipe with viscoelastic coatings applied. Furthermore, the wave structure was calculated for various roots to verify that the boundary conditions were met and to explore the attenuation characteristics of some of the modes. To obtain experimental results, test samples were fabricated out of 4 in. Schedule 40 (0.25 in. wall thickness) steel pipes and were coated with a commercial bitumen pipe coating. Guided-wave tests were performed with arrays of piezoelectric transducers and wedges positioned circumferentially around the pipe for comparison to the theoretical results.

A. Dispersion Curves

Fig. 2 shows the phase velocity and attenuation dispersion curve calculations for a 4 in. Schedule 40 steel pipe, coated with 0.020 in. of viscoelastic Emerson and Cumming, 2057—Cat 9 epoxy (Emerson & Cumming, Billerica, MA). Temporarily, limiting the discussion to the phase-velocity dispersion curve, the first and most obvious comment is that it looks similar to that of the single-layer, elastic, hollow-cylinder case, as published in many references. At low frequency, two modes exist, *L(0,1)* and *L(0,2)*, the notation being consistent with the classical notation for longitudinal guided waves in single-layer, elastic, hollow cylinders. The *L(0,2)* mode has a cutoff frequency at about 35 kHz, below which the mode does not exist. As the frequency increases past the cutoff frequencies for various modes, they enter the dispersion curve at high-

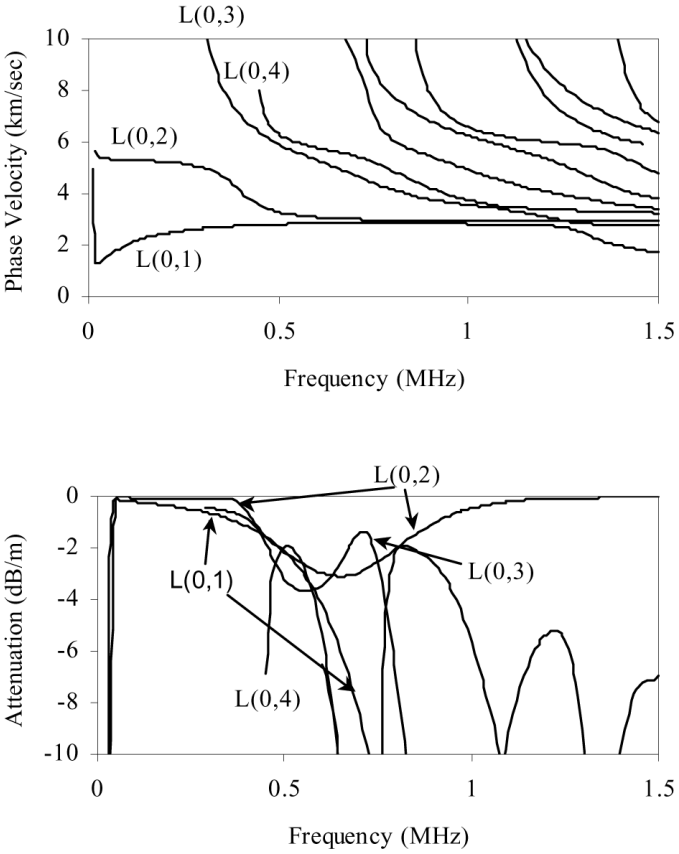

Fig. 2. Phase velocity and attenuation dispersion curves for a two-layer structure consisting of a 4 in. Schedule 40 steel pipe, coated with a 0.020 in. layer of E&C 2057—Cat 9 epoxy, with the first four modes labeled *L(0,1)–L(0,4)*. Considering that the wave guide is made up primarily of the steel pipe, it is not surprising that the phase-velocity dispersion curve closely resembles that of the single-layer elastic wave guide. The attenuation dispersion curve shows the general trend of increasing attenuation with increasing frequency, with the addition of some very interesting modal points where low attenuation occurs.

phase velocity and most seem to approach the shear wave, or surface wave velocity of the elastic material as the frequency increases. However, the *L(0,1)* and *L(0,4)* modes break away below the surface wave velocity of the elastic material, which is inconsistent with the single-layer, elastic case, in which these modes would normally approach the surface and shear wave velocities of the elastic material. The other subtle difference in the multilayer dispersion curve as compared to the single-layer, elastic curves is the positioning of the modes and the location and existence of mode crossings. These appear to change based upon the exact make up of the wave guide.

Now, considering the attenuation dispersion curve, some interesting mode attenuation behavior can be observed. The lowest order modes, *L(0,1)* and *L(0,2)*, at very low frequency, have low attenuation, except for the cutoff region of the modes in which a jump is seen in the attenuation curve. In general this low-attenuation, low-frequency behavior is the expected result because the attenuation constant increases with frequency for conventional bulk longitudinal and shear wave propagation.

As the *L(0,1)* mode increases in frequency, the attenuation increases slightly then decreases, approaching zero attenuation. Theoretically, for a mode to have a zero attenuation value, all of the energy must be propagating in the elastic medium only. Because the phase velocity for this mode is approaching the surface wave velocity, it is likely that this zero attenuation mode is actually a surface wave traveling on the inside diameter of the pipe. Conversely, the *L(0,1)* modes appear to be approaching very large attenuation values as frequency increases. This should indicate that the wave mode is traveling primarily in the viscoelastic layer as the frequency increases.

As frequency increases past the cutoff frequency of various modes, these new modes appear on the dispersion curves. On the attenuation dispersion curve, the attenuation values tend to begin at large values near the cutoff frequency, then approach one or more local minimum attenuation values and diverge toward high-attenuation values.

The attenuation dispersion curves have some interesting implications on the mode selection for flaw detection in coated pipes. The principle result is that all of the modes show drastic changes in attenuation over the frequency range of interest. Thus, the attenuation dispersion curve is critical for performing an ultrasonic test. Knowledge of the attenuation dispersion curve will allow the generation of low attenuation modes by changing incident angle and frequency.

Ultimately, a particular mode, or modes, will have to be chosen that have an acceptable level of attenuation as based upon the length of propagation and the available signal to noise of the test. As an example, a guided-wave test will have some signal-to-noise ratio based upon the size of the reflection from the flaw as compared to the electronic and acoustic noise level of the system. Obviously, this level varies with the size of flaw, but a realistic value for this example is a flaw signal 40 dB above the noise. Furthermore, it is reasonable to specify that the minimum signal to noise of the test must be 6 dB. Thus, there is 34 dB of signal that can be lost due to attenuation of the guided-wave mode. If in this example the ultimate goal is to test 10 m of the pipe with a single transducer placement, meaning that the wave will have to travel a total of 20 m, a suitable mode must be chosen that has less than -1.7 dB/m of attenuation at the maximum. Possible modes for the epoxy-coated pipe would be the *L(0,1)* and *L(0,2)* modes below 500 kHz, the *L(0,3)* mode at 300–400 kHz and at 700 kHz. If more signal to noise is available or the propagation distance is shorter, the *L(0,4)* and *L(0,5)* modes have low attenuation points at approximately -2 to -3 dB/m that may be useful for inspection.

B. Wave Structure

It is desirable to make some checks on the numerical solution of the dispersion equation to verify that the dispersion curves are correct. Obviously, one indication that the curves are reasonable is simply that the phase and

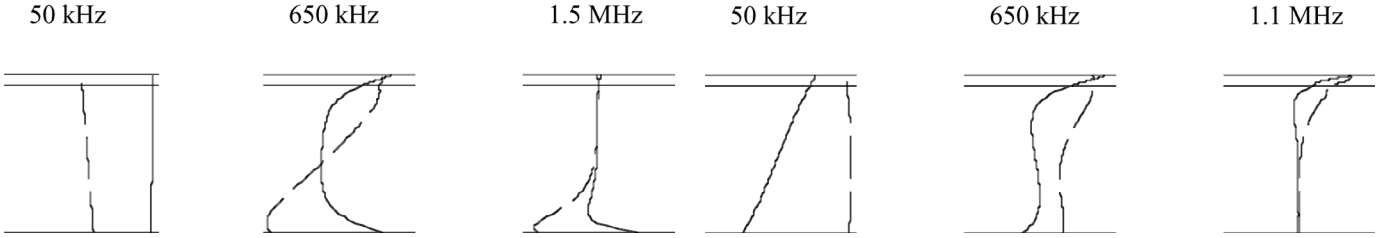

Fig. 3. Normalized displacement wave structure for the *L(0,2)* mode in a 4 in. Schedule 40 steel pipe coated with 0.020 in. of E&C 2057 epoxy. Mode shapes at three frequencies are shown that correspond to points of minimum attenuation at 50 kHz and 1.5 MHz and a point of maximum attenuation at 650 kHz. The mode shape at 1.5 MHz is consistent with surface wave propagation on the inside diameter of the pipe. Note that the solid line corresponds to the in plane displacement component, u_z, and the dashed line corresponds to the out-of-plane displacement component, u_r.

Fig. 4. Normalized displacement wave structure for the *L(01)* mode in a 4 in. Schedule 40 steel pipe coated with 0.020 in. of E&C 2057 epoxy. Mode shapes at three frequencies are shown that correspond to points of increasing attenuation from 50 kHz to 1.1 MHz. Note that the solid line corresponds to the in plane displacement component, u_z, and the dashed line corresponds to the out-of-plane displacement component, u_r.

group velocity dispersion curves look similar to the single-layer, elastic curves. However, beyond this reasoning, some numerical means should be used to verify that the roots have been solved correctly. Because the dispersion equations are based upon a boundary value problem, the most logical way to verify that the roots have been solved correctly is to make sure that the boundary conditions and interfacial continuity equations have been satisfied. To accomplish this, the wave structure of the propagating modes can be examined.

A plot of the wave structure for a guided-wave mode is simply a plot of the displacement and stress components across the thickness of the wave guide. To do this, the root of the guided-wave mode of interest must be substituted into the appropriate equations for the displacements and stresses. The only additional process that must be done before plotting the values is to generate the unknown amplitude constants. This is simply done by setting one of the unknown constants equal to unity, and rearranging the global matrix to solve for the additional constants.

From the wave structure curves, it is possible to check the boundary conditions on the stress at the free surfaces and the continuity of stress and displacement at the interfaces. Furthermore, it is interesting to check the proportionality of stress and displacement between the elastic and viscoelastic layers. For low attenuation modes, it is expected that the elastic layer will carry a high proportion of the stress and displacement, and for high-attenuation modes, the viscoelastic layer should carry a high proportion of the stress and displacement.

Two modes were examined because of their interesting attenuation behavior. First, the wave structure for the *L(0,2)* mode was calculated. The attenuation behavior is interesting in that it starts at a very low value, less than -1 dB/m, then increases to a maximum of approximately -3 dB/m at 650 kHz, then decreases, approaching zero attenuation at high frequency. The displacement wave structure for three frequencies is displayed in Fig. 3. The progression of wave structure changes appears consistent with the attenuation dispersion curve for this mode. Furthermore, the displacement boundary conditions are shown to be satisfied (the stress boundary conditions also were checked but they are not displayed here). Based on the velocity and attenuation of the *L(0,2)* mode at 1.50 MHz, it was suggested that this mode is a surface wave propagating on the inside diameter of the pipe. The wave structure that is plotted at 1.5 MHz in Fig. 3 is completely consistent with surface wave propagation, as compared with published sources of surface wave displacement characteristics [28]–[31].

The second mode that was examined is the *L(0,1)* mode. The attenuation of this mode begins at a low value at low frequency and diverges rapidly toward very large values at high frequency. The wave structure is displayed in Fig. 4. Unlike the previous mode, as the frequency increases the proportion of energy propagating in the viscoelastic layer increases. In fact, the wave structure appears to be displaying surface wave propagation on the outside diameter of the viscoelastic layer.

C. Experimental Results on a Coated Pipe

An experiment was designed to obtain results that would verify the attenuation dispersion curves for a coated pipe. A test sample was fabricated from a length of 4 in. Schedule 40 steel pipe by coating it with a commercial bitumen coating material per the manufacturer's instructions. The thickness of the coating was measured to be approximately 0.006 in. on average across the test specimen. Guided waves were generated in the test specimen by using the angle of incidence principle. In order to generate axially symmetric modes, an array of 8 to 10 transducer/wedge pairs were positioned around the circumference of the pipe. In total, three transducer/wedge pairs were used to generate the *L(0,2)* mode at approximately 180 kHz, the *L(0,1)* mode at approximately 600 kHz, and the *L(0,3)* mode at approximately 750 kHz. Fig. 5 shows the *L(0,2)* and *L(0,3)* arrays applied to two of the test specimens. A Matec Explorer II (Matec Instruments, Northborough, MA) tone burst system was used to operate the transducer arrays and perform data collection.

The phase velocity and attenuation dispersion curves are shown in Fig. 6 for the bitumen-coated test sample. Experimental data points that were obtained using the

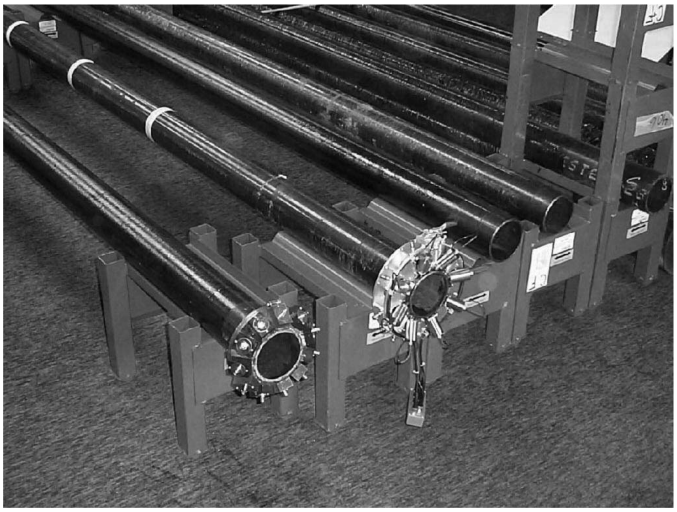

Fig. 5. Photograph of two of the transducer arrays that were used in obtaining experimental attenuation values on the coated test specimens.

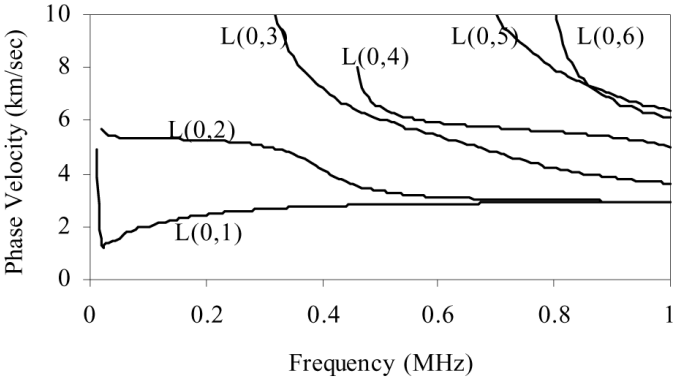

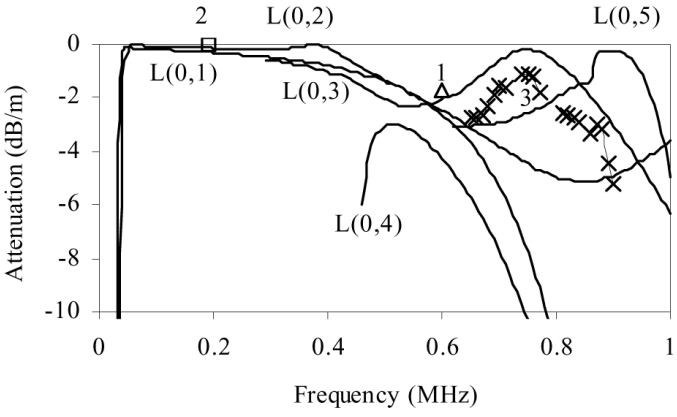

Fig. 6. Phase velocity and attenuation dispersion curves for a two-layer structure consisting of a 4 in. Schedule 40 steel pipe, coated with a 0.006 in. layer of a commercial bitumen pipe coating, with the modes labeled *L(0,1)–L(0,6)*. Experimental data points that were generated with three transducer arrays are displayed on the attenuation dispersion curve, showing very good agreement between the numerical and experimental results. Experimental results are for the *L(0,1)*, *L(0,2)*, and *L(0,3)* modes are marked with a square, triangle, and "x" and are labeled 1, 2, and 3, respectively.

three transducer arrays are plotted along with the numerical result for the attenuation dispersion curve. Single data points are shown for the *L(0,1)* mode at 600 kHz (labeled 1), and for the *L(0,2)* mode at 180 kHz (labeled 2). A series of data points was taken for the *L(0,3)* mode between 650 and 900 kHz (labeled 3). The experimental points agree well with the attenuation dispersion curve.

IV. Conclusions

The presence of attenuative, viscoelastic coatings cause significant problems for developing a guided-wave, nondestructive inspection of coated pipes. However, the multimode nature of guided waves offers the potential for finding modes that will perform even in the presence of these coatings. For the purpose of finding these modes, a multilayer, hollow cylinder model that includes viscoelastic layers was developed using the global matrix method to describe the longitudinal modes of propagation. The numerical solution of the model yields attenuation dispersion curves which clearly show that, by changing the mode and frequency of operation, low attenuation behavior can be obtained, even for the higher order modes at relatively high frequency. These modes offer an alternative to only using the lowest order modes at very low frequencies to perform an inspection. Wave structure and experimental results were used to verify the accuracy of the theoretical model. The wave structure showed that the boundary conditions had been satisfied and offered insight into the attenuation behavior for the two lowest order modes. The experimental results showed good agreement with the theoretical dispersion curve, giving confidence to the use of the theoretical model for developing a nondestructive test.

References

[1] M. G. Silk and K. F. Bainton, "The propagation in metal tubing of ultrasonic wave modes equivalent to Lamb waves," *Ultrasonics*, vol. 17, pp. 11–19, 1979.

[2] R. B. Thompson, G. A. Alers, and M. A. Tennison, "Applications of direct electromagnetic Lamb wave generation to gas pipeline inspection," in *Proc. IEEE Ultrason. Symp.*, 1972, pp. 91–94.

[3] J. L. Rose, D. Jiao, and J. Spanner, Jr., "Ultrasonic guided wave NDE for piping," *Mater. Eval.*, vol. 54, pp. 1310–1313, 1996.

[4] D. Alleyne and P. Cawley, "The excitation of Lamb waves in pipes using dry-coupled piezoelectric transducers," *J. Nondestructive Eval.*, vol. 15, pp. 11–20, 1996.

[5] J. Ditri, J. L. Rose, and G. Chen, "Mode selection criterion for defect detection optimization using Lamb waves," *Rev. Progr. Quantitative Nondestructive Eval.*, vol. 11, pp. 2109–2115, 1991.

[6] J. N. Barshinger, "Guided waves in pipes with viscoelastic coatings," Ph.D. dissertation, The Pennsylvania State University, State College, PA, 2001.

[7] J. N. Barshinger and J. L. Rose, "Ultrasonic guided wave propagation in pipes with viscoelastic coatings," *Rev. Progr. Quantitative Nondestructive Eval.*, vol. 21A, pp. 239–246, 2001.

[8] J. N. Barshinger, J. L. Rose, and M. J. Avioli, "Guided wave resonance tuning for pipe inspection," *J. Pressure Vessel Technol.*, vol. 124, pp. 303–310, 2002.

[9] J. Rayleigh, *The Theory of Sound, vol. I and II.* New York: Dover, 1945.

[10] H. Lamb, "On waves in an elastic plate," *Proc. R. Soc. London*, vol. A93, 1917, p. 114.
[11] L. Pochhammer, "Uber die fortpflanzungsgeschwindigkeiten kleiner schwingungen in einem unbegrenzten isotropen kreiscylinder," *J. fur Math.*, vol. 81, pp. 324–336, 1876 (Crelle). (in German)
[12] C. Chree, "Longitudinal vibrations of a circular bar," *Q. J. Math.*, vol. 21, pp. 287–298, 1886.
[13] A. Love, *A Treatise on the Mathematical Theory of Elasticity*. New York: Dover, 1944.
[14] T. Lin and G. Morgan, "A study of axisymmetric vibrations of cylindrical shells as affected by rotatory inertia and transverse shear," *J. Appl. Mech.*, vol. 78, pp. 255–261, 1956.
[15] R. M. Cooper and P. M. Naghdi, "Propagation of nonaxially symmetric waves in elastic cylindrical shells," *J. Acoust. Soc. Amer.*, vol. 29, pp. 1365–1373, 1957.
[16] I. Mirsky and G. Herrmann, "Axially symmetric motions of thick cylindrical shells," *J. Appl. Mech.*, vol. 80, pp. 97–102, 1958.
[17] G. Herrmann and I. Mirsky, "Three-dimensional and shell-theory analysis of axially symmetric motions of cylinders," *J. Appl. Mech.*, vol. 78, pp. 563–568, 1956.
[18] D. C. Gazis, "Three-dimensional investigation of the propagation of waves in hollow circular cylinders. I. Analytical foundation," *J. Acoust. Soc. Amer.*, vol. 31, pp. 568–573, 1959.
[19] D. C. Gazis, "Three-dimensional investigation of the propagation of waves in hollow circular cylinders. II. Numerical results," *J. Acoust. Soc. Amer.*, vol. 31, pp. 573–578, 1959.
[20] W. T. Thomson, "Transmission of elastic waves through stratified solid medium," *J. Appl. Phys.*, vol. 21, pp. 89–93, 1950.
[21] N. A. Haskell, "Dispersion of surface waves on multilayered media," *Bull. Seismological Soc. Amer.*, vol. 43, pp. 17–34, 1953.
[22] L. Knopoff, "A matrix method for elastic wave problems," *Bull. Seismological Soc. Amer.*, vol. 54, pp. 431–438, 1964.
[23] B. Hosten, "Bulk heterogeneous plane waves propagation through viscoelastic plates and stratified media with large values of frequency domain," *Ultrasonics*, vol. 29, pp. 445–450, 1991.
[24] D. Levesque and L. Piche, "A robust transfer matrix formulation for the ultrasonic response of multilayered absorbing media," *J. Acoust. Soc. Amer.*, vol. 92, pp. 452–467, 1992.
[25] P. Kielczynski and J. D. N. Cheeke, "Love wave propagation in viscoelastic media," in *Proc. IEEE Ultrason. Symp.*, 1997, pp. 437–440.
[26] M. J. S. Lowe, "Matrix techniques for modeling ultrasonic waves in multilayered media," *IEEE Trans. Ultrason., Ferroelect., Freq. Contr.*, vol. 42, pp. 525–542, Jul. 1995.
[27] I. A. Viktorov, *Rayleigh and Lamb Waves*. New York: Plenum, 1967.
[28] K. F. Graff, *Wave Motion in Elastic Solids*. New York: Dover, 1991.
[29] J. D. Achenbach, *Wave Propagation in Elastic Solids*. New York: Elsevier, 1975.
[30] B. A. Auld, *Acoustic Fields and Waves in Solids*. vol. II, Wiley Interscience, 1973.
[31] J. L. Rose, *Ultrasonic Waves in Solid Media*. Cambridge, UK: Cambridge Univ. Press, 1999.
[32] W. Ewing, W. Jardetsky, and F. Press, *Elastic Waves in Layered Media*. New York: McGraw-Hill, 1957.
[33] G. C. Gaunaurd and M. F. Werby, "Acoustic resonance scattering by submerged elastic shells," *Appl. Mech. Rev.*, vol. 43, pp. 171–208, 1990.
[34] G. C. Gaunaurd, "Sonar cross section of a coated hollow cylinder in water," *J. Acoust. Soc. Amer.*, vol. 60, pp. 360–368, 1977.
[35] R. M. Christensen, *Theory of Viscoelasticity: An Introduction*. New York: Academic, 1981.
[36] R. H. Blanc, "Transient wave propagation methods for determining the viscoelastic properties of solids," *J. Appl. Mech.*, vol. 60, pp. 763–768, 1993.
[37] P. J. Torvik, "Reflection and wave trains in semi-infinite plates," *J. Acoust. Soc. Amer.*, vol. 41, pp. 346–353, 1967.
[38] O. Diligent, M. J. S. Lowe, E. Le Clezio, M. Castaings, and B. Hosten, "Prediction and measurement of non-propagating Lamb modes at the free end of a plate when the fundamental antisymmetric mode a0 is incident," *J. Acoust. Soc. Amer.*, vol. 113, pp. 3032–3042, 2003.

James N. Barshinger (M'02) was born in Wilkes-Barre, PA, in 1972. He received his graduate and undergraduate degrees from The Pennsylvania State University, University Park, PA, in engineering science and mechanics (B.Sc., 1995), (M.Sc., 1997), and (Ph.D., 2001). He is currently a research scientist in the Non-Destructive Technologies Laboratory at The General Electric Company, Global Research Center, Schenectady, NY.

His primary research efforts have been focused on ultrasonic nondestructive testing, including conventional ultrasonic techniques, guided wave, and ultrasonic phased array. He was previously employed at Agfa NDT Inc., Krautkramer Ultrasonic Systems, Lewistown, PA, as a transducer development engineer, where his primary efforts involved the design of ultrasonic phased-array transducers for industrial nondestructive testing.

Dr. Barshinger is a member of the American Society for Non-Destructive Testing.

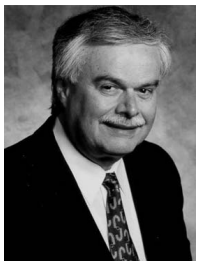

Joseph L. Rose (M'74) is the Paul Morrow Professor in Design and Manufacturing, Department of Engineering Science and Mechanics at The Pennsylvania State University, University Park, PA. He is the author of over 10 patents, four textbooks, and over 350 articles on ultrasonic nondestructive evaluation (NDE), wave mechanics, medical ultrasound, adhesive bonding, concrete inspection, pipe and tubing inspection, and composite material inspection. Textbooks include *Basic Physics in Diagnostic Ultrasound* (John Wiley & Sons, Inc., New York, 1979) and *Ultrasonic Waves in Solid Media* (Cambridge University Press, Cambride, UK, 1999). He has served as principal advisor to over 40 Ph.D. students. Current research activity is directed toward wave mechanics, aging aircraft inspection, tubing and piping inspection for the power generation and chemical processing industries, and hidden corrosion detection.

Dr. Rose received his Ph.D. degree from Drexel University, Philadelphia, PA, in 1969.

He received a variety of awards, including American Society for Nondestructive Testing Paper of the Year achieved in 1973; Fellowship Award in 1985, 1997, and 2000; Tutorial Citation Award in 1986; and Fellow in 2000. He also received several university teaching and research awards. Dr. Rose was a finalist in the 1995 Discover Awards for technological innovation in Aviation and Aerospace for the development of a hand-held probe for aging aircraft inspection. He was the recipient of a University Faculty Scholar medal for achievement in engineering in 1996 and an outstanding research award in 1997.

Dr. Rose is a fellow of the American Society for Nondestructive Testing and the American Society of Mechanical Engineers.